Low-Voltage Syngas Synthesis via BPM Electrolysis of CO_2 Capture and Aldehyde Solution

Po-Wei Huang[1]†, Hyeonuk Choi[2]†, Anush Venkataraman[1], Olivia Vulpin[3], Claudio A. Ruiz Torres[4], Danae A. Chipoco Haro[5], Yaguang Zhu[4], Erika R. Yamazaki[1], Kelsey B. Hatzell[4], Shannon W. Boettcher[3,6,7], Sankar Nair[1], Jihun Oh[2]*, Hakhyeon Song[8]*, Marta C. Hatzell[1,8]*

Affiliations:

[1]School of Chemical and Biomolecular Engineering, Georgia Institute of Technology, Atlanta, GA 30332, USA.
[2]Department of Materials Science and Engineering, Korea Advanced Institute of Science and Technology (KAIST), Daejeon 34141, Republic of Korea.
[3]Department of Chemistry and Biochemistry, Oregon Center for Electrochemistry, University of Oregon, Eugene, Oregon 97403, United States.
[4]Andlinger Center for Energy and the Environment, Princeton University, Princeton, New Jersey 08540, United States.
[5]School of Materials Science and Engineering, Georgia Institute of Technology, Atlanta, Georgia 30332, United States.
[6]Department of Chemical & Biomolecular Engineering and Department of Chemistry, University of California, Berkeley, California 94720, United States
[7]Energy Storage and Distributed Resources Division, Lawrence Berkeley National Laboratory, Berkeley, California 94720, United States
[8]George W. Woodruff School of Mechanical Engineering, Georgia Institute of Technology, Atlanta, Georgia 30332, United States.

***Corresponding author. Email: jihun.oh@kaist.ac.kr (J. O.); hakhyeon.song@me.gatech.edu (H. S.) marta.hatzell@me.gatech.edu (M. C. H.)**
†These authors contributed equally to this work.

Abstract

We demonstrate an electrochemical syngas production platform that couples bicarbonate electrolysis with formaldehyde oxidation in a bipolar membrane electrode assembly. This strategy doubles syngas ($CO + H_2$) throughput compared to conventional CO_2 electrolysis by generating CO at the cathode and H_2 at the anode. The system achieves a full-cell voltage of 1.7 V while operating at an industrially relevant current density of 200 mA cm^{-2}. The system maintained a combined Faradaic efficiency of 200% over 8 hours. The process produces gas with a 1:1 H_2:CO ratio, aligning with downstream requirements for Fischer-Tropsch synthesis. We further investigated how Cu anode active sites and electrolyte composition affect formaldehyde oxidation activity. Our integrated electrolytic system reduces levelized energy by 45% to 61% relative to conventional electrochemical syngas production platforms.

Introduction

Carbon monoxide (CO) is a key building block in chemical and fuel production.[1] Analysts project that the global CO market will grow at a compound annual growth rate (CAGR) of 4.4% over the next decade.[2] The current industrial production of CO depends on fossil-based resources and carries a high carbon footprint (0.57 $t_{CO2\text{-}e}$ t_{CO}^{-1}).[1] Switching the feedstock to CO_2 through CO_2 electrolysis (CO_2E) offers a promising cleaner alternative for CO generation.[3-5] Industry widely considers CO the most viable electrochemical commodity chemical derived from CO_2 because CO forms through a simple two-electron reaction, requires a low activation overpotential, and has strong market demand.[6-8] This demand is expected to further increase with the global push for carbon neutrality. For instance, projections for sustainable aviation fuels growth indicate that at least 300 Mt of CO are needed by 2050, approximately double the current annual production for CO.[9,10] Despite the need for CO, pure CO alone is generally incompatible with most industrial processes and typically needs to be mixed with hydrogen (H_2) to form syngas. The optimal H_2:CO ratio varies by application (**Fig. 1A**). Process such as the Fischer-Tropsch (F-T) method requires syngas with a ratio between 1 and 2 to produce liquid fuels.[11] The global syngas market is predicted to increase more than fivefold, reaching 670 Mt by 2050.[9]

Electrochemical syngas production currently employs two primary approaches (**Fig. 1B**). The first uses a single CO_2 electrolyzer where H_2 and CO are co-produced at the cathode via catalysts with moderate CO selectivity.[12,13] The second couples a CO_2 electrolyzer with a water electrolyzer to produce CO and H_2 independently.[9] As water electrolyzer technology is more mature and typically operates at lower voltages (1.8–2.0 V) than CO_2 electrolyzers ($\geq$ 2.5 V), producing H_2 via water electrolysis requires less energy in the dual-cell configuration, albeit with higher capital cost and system complexity.[9,14] While the economic preference remains under debate, both configurations are theoretically limited to a syngas molar yield per coulomb of

0.00517 mmol C^{-1}, as the anodic oxygen evolution reaction (OER) does not contribute to syngas formation. Moreover, the high thermodynamic potential (1.23 V vs RHE, V_{RHE}) and slow kinetics of the OER elevate the cell voltage.[5,15] Such high-voltage operation increases energy costs and accelerates material degradation, compromising practical viability.[16,17] Efforts to address this have focused on improving anode materials or replacing OER with lower-potential reactions.[18-20] On the cathode side, gaseous CO_2E requires high-purity CO_2 and suffers from low CO_2 utilization ($\leq$ 50%).[5,21] In contrast, bicarbonate electrolysis (BCE) offers improved CO_2 utilization and readily integrates with carbon capture technologies, making BCE a promising alternative.[22,23] One limitation of BCE is the additional voltage losses incurred due to the thermodynamic potential of water dissociation (0.83 V), along with the overpotential required to drive the kinetics of water dissociation in the bipolar membrane (BPM).[24] As a result, BCE often exhibits even higher cell voltages than gaseous CO_2E under comparable conditions, exceeding 3.8 V at industrially relevant current densities ($\geq$ 200 mA cm^{-2}) which is not practical.[14]

Recent interest in aldehyde oxidation reactions presents a unique opportunity for electrochemical syngas production when coupled with BCE. In addition to offering a low thermodynamic potential, approximately 1.45 V lower than that of OER (**Fig. S1**), aldehyde oxidation enables anodic H_2 generation, a process traditionally considered unfeasible in electrochemical systems. The anodic H_2 production is considered to involve C–H bond cleavage of the aldehyde group followed by surface hydrogen recombination (Tafel step). Previous studies on Cu-based aldehyde oxidation, employing in-situ spectroscopy, operando differential electrochemical mass spectroscopy (DEMS) measurements, and DFT calculations, have provided evidence for the feasibility of such hydrogen recombination pathways under low overpotential conditions.[25-27] Our Tafel slope and reaction order analyses are kinetically consistent with a hydrogen recombination-influenced pathway (**Supplementary Text 1**).

In this work, we demonstrate a single-reactor approach for syngas production by integrating BCE with formaldehyde oxidation reaction (FOR) in a BPM-based membrane electrode assembly (MEA). With both electrodes contributing to syngas component (CO and/or H_2) generation, the system achieves a theoretical molar yield per coulomb of 0.01034 mmol C^{-1}, double that of conventional configurations. We investigate the correlation between FOR activity and the material properties of the Cu anodes and further identify the crucial role of electrolyte composition (mixture of HCHO and KOH) in sustaining anodic hydrogen production at elevated current densities (up to 600 mA cm^{-2}). We demonstrate a full-cell operation of 1.7 V at 200 mA cm^{-2}, while maintaining Faradaic efficiency (FE) for CO generation at the cathode and H_2 generation at the anode both around 100% over 8 hours electrolysis. The combined gas streams from both electrodes exhibit an H_2:CO ratio near 1, making the output directly applicable as syngas for industrial use. Energy analysis indicates that the levelized energy requirement of the BCE-FOR electrolyzer is 3.2 MWh ton^{-1}_{syngas}, which is 45% and 61% lower than that of conventional electrochemical syngas production based on gaseous CO_2E-OER and BCE-OER, respectively. While the BCE-FOR system still requires more energy than petrochemical routes, it possesses the advantage of producing tunable H_2:CO ratios by adjusting the applied current density, with value as low as unity within a single reactor, which is not achievable through traditional petrochemical processes. With continued advances in balance-of-plant (BoP) components, BCE-FOR holds the potential to become a viable approach for CO_2-derived syngas production.

Results and Discussion

Integration of FOR and BCE in BPM-MEA

To realize full-cell electrochemical syngas production, we integrated BCE with FOR in a BPM-MEA configuration (**Fig. 2A**), where a bicarbonate solution (3 M $KHCO_3$) is converted to CO at

the cathode and a formaldehyde solution (1 M HCHO + 1 M KOH) is oxidized at the anode to generate H_2 and formate. Operating the BPM in reverse-bias mode induces a locally acidic environment at the cathode-BPM interface, converting bicarbonate to gaseous CO_2 near the catalyst surface.[22] The *in-situ* generated CO_2 is then reduced to CO, enabling direct use of bicarbonate solutions commonly regarded as electrochemically inert (**Supplementary Text 2**). For selective and stable CO production under these conditions, we employed a Ni single-atom catalyst (Ni-SAC) at the cathode, which exhibits high activity and durability under BPM conditions (**Figs. S2–S4**).[14,28] At the anode, we used a pretreated Cu foam (Cu/Cu_2O electrode, **Figs. S5–S7**), as Cu-based materials have been reported to exhibit activity toward aldehyde oxidation reactions.[25,29,30] The reactor produces only CO and H_2, with an H_2:CO ratio of 1.0 to 2.1 across current densities from 100 to 600 mA cm^{-2} (**Fig. 2B**), making the gas products well-suited as syngas for downstream applications such as the F-T process. For comparison, BCE-OER using commercial Ni foam as the anode for OER yielded low H_2:CO ratios (0 to 0.9), reflecting the inherent trade-off in CO_2E studies between achieving high CO selectivity and producing syngas with application-relevant H_2:CO ratios. Although higher current densities can promote HER and thereby shift the H_2:CO ratio toward more favorable values (e.g., 0.9 at 600 mA cm^{-2} in our system), this strategy compromises energy consumption due to increased whole-cell overpotential. The BCE-FOR system, with both electrodes contributing to syngas component (CO and/or H_2) generation, achieved a comparable CO + H_2 throughput at 300 mA cm^{-2}, requiring only half the current for BCE-OER setup (600 mA cm^{-2}; **Fig. 2C**).

The total CO + H_2 production in the BCE-FOR system began to decline when the current exceeded 400 mA cm^{-2}. At 600 mA cm^{-2} the production rate was only 85% of the theoretical value (**Fig. 2C**). This trend was not observed in the BCE-OER system. The decrease in total syngas output can be attributed to the reduction in anodic performance, while the cathode remained stable

under these experimental conditions (**Fig. 2B** and **Fig. S8**). No O_2 was detected in the BCE-FOR system, indicating that OER did not occur as a competing reaction at anode. Furthermore, although a trace amount of CO_2 was detected, suggesting the potential for deep oxidation of HCHO, formate, or methanol, its contribution is practically negligible within our operating current density range (**Supplementary Text 3**). Additionally, inductively coupled plasma optical emission spectroscopy (ICP-OES) analysis confirmed that the anodic dissolution of the Cu catalyst is strictly negligible (0.048 ppm), demonstrating robust structural stability without metal leaching (**Supplementary Text 3**). Instead, post-electrolysis characterization revealed partial oxidation of the anode surface, with visibly darkened regions (**Fig. S9B**). X-ray photoelectron spectroscopy (XPS) analysis showed a transition from the original doublet peaks indicative of mixed-valence states (Cu^0 + Cu^+) in the fresh Cu/Cu_2O electrode, to predominantly oxidized Cu species (Cu^+/Cu^{2+}) after electrolysis, with the Cu^0 signal nearly disappearing (**Fig. S10**). Despite the change in valence states, the electrode morphology remained unchanged (**Fig. S11**). These observations suggest that localized oxidation occurs at high current densities and may contribute to the degradation of anodic activity.

The instability of Cu-based electrodes has been reported;[27,31,32] however, our results show that the Cu/Cu_2O electrode remains stable under moderate current densities, as demonstrated by five consecutive 30-minute electrolysis tests at 200 mA cm^{-2} (**Fig. S12–14**). The observed Cu oxidation is likely triggered by increased overpotentials associated with mass transport limitations during high rate FOR operation. This phenomenon cannot be attributed to HCHO depletion, as similar discoloration (**Fig. S9C**) and reduced gas production (**Fig. 2C**) were observed when the HCHO concentration was doubled (2 M HCHO + 1 M KOH). Surprisingly, increasing the KOH concentration while maintaining the HCHO level (1 M HCHO + 2 M KOH) restored the total CO + H_2 production rate to values consistent with theoretical predictions and mitigated catalyst degradation (**Fig. S9D**). These findings underscore the need for a deeper understanding of the

active sites on the Cu/Cu_2O electrode and the influence that the electrolyte composition has on the FOR performance.

Evaluating Cu Active Sites for FOR

Although Cu-based electrodes are commonly used for studying aldehyde oxidation reactions, which Cu sites are active is not conclusively established. The prevailing hypothesis suggests that the Cu valence state plays a key role, with metallic Cu (Cu^0) being the primary active site.[25,29] However, the role of Cu oxides, especially Cu^+, is still debated.[26,31]

To investigate the FOR active sites on Cu, we first performed linear sweep voltammetry (LSV) in an H-cell using 1 M KOH with and without HCHO (**Fig. 3A**). In the presence of HCHO, a current response appeared starting at –0.1 V_{RHE} and plateaued near 0.4 V_{RHE}, indicative of FOR. In contrast, no significant current was observed in the absence of HCHO until 0.5 V_{RHE}, corresponding to Cu oxidation (Cu^0 to Cu^+). We then prepared four electrodes (Cu, Cu/Cu_2O, Cu_2O, and CuO) each with distinct valence states confirmed by Auger XPS (**Fig. 3B**) and evaluated their activity via chronoamperometry (CA) at 0.39 V_{RHE}. This potential was selected based on LSV (**Fig. 3A**) to avoid interference from further Cu oxidation. Only the Cu/Cu_2O electrode exhibited intrinsic activity (7.90 mA cm^{-2}_{ECSA}) toward FOR, while Cu, Cu_2O, and CuO electrodes were inactive (**Fig. 3C**). Notably, the electrochemical surface area (ECSA) of the Cu/Cu_2O electrode was an order of magnitude higher than that of the other three electrodes (**Fig. S15, 16, and Table S1**). To decouple the influence of surface area, a pulse-treated Cu electrode was prepared by subjecting fresh Cu foam to pulsing cycles,[33] which introduced mixed valence states while preserving a similar ECSA (**Fig. S17 and S18**). Despite the pulse-treated Cu foam and pristine Cu exhibited ECSA within the same order of magnitude, only the pulse-treated sample showed measurable FOR activity (8.58 mA cm^{-2}_{ECSA}; **Fig. S19**). Our results suggest that well-dispersed hybrid valence states (Cu^0 and Cu^+) are essential for FOR, while bulk forms containing only Cu^0

or Cu^+ exhibit negligible activity. These synergistic effects are in line with earlier studies,[34] which show that mixed-valence Cu electrodes enhance aldehyde adsorption relative to their single-valence (Cu^0 or Cu^+) counterparts. Furthermore, during the stability test, five consecutive CA cycles yielded stable H_2 production and no observable change in the valence state of the Cu/Cu_2O electrode when the applied voltage was kept below the Cu oxidation potential (**Fig. S20**). In contrast, operation at a voltage above the Cu oxidation potential led to complete oxidation of the Cu electrode and a H_2 FE of 0% (**Fig. S21**), indicating that the observed current was predominantly due to Cu oxidation and associated with catalytic deactivation. These results align with our MEA findings and suggest that operating below the Cu oxidation onset potential is key to maintaining the hybrid valence states (Cu^0 and Cu^+), which is critical for sustained FOR activity on the Cu/Cu_2O electrode.

Influence of Electrolyte Composition on FOR

To investigate the influence of electrolyte on FOR, we measured the response current, as a proxy for FOR activity, at 0 V_{RHE} across a range of electrolyte compositions (50–2000 mM KOH and 50–1000 mM HCHO) in an H-cell. 0 V_{RHE} was selected as it is below the onset potential of Cu oxidation (approximately 0.5 V_{RHE}), ensuring that the current arises solely from FOR. The response current, and thus FOR activity, varied significantly with electrolyte composition (**Fig. 4A**). At a fixed HCHO level, FOR activity increased monotonically with KOH concentration. However, when KOH concentration was held constant, FOR activity followed a volcano-like trend with respect to HCHO concentration, initially increasing and then declining. These findings are consistent with MEA results (**Fig. 2C**). When FOR activity becomes limited (≥400 mA cm^{-2} in 1 M KOH with 1 M HCHO), further increases in HCHO concentration (1 M KOH with 2 M HCHO) lead to a decline in performance. In contrast, enhancing the KOH concentration under the same

HCHO condition (2 M KOH with 1 M HCHO) improves FOR activity, mitigates the overpotential, and enables operation at higher current densities (**Fig. S22**).

$$2HCHO + 4OH^- \rightarrow 2HCOO^- + H_2 + 2H_2O + 2e^- \text{ (**Equation 1**; electrochemical reaction)}$$

$$2HCHO + OH^- \rightarrow HCOO^- + CH_3OH \text{ (**Equation 2**; chemical reaction)}$$

We further probed the volcano-type trend in FOR activity with varying HCHO concentrations. Similar patterns have been reported in previous studies[29] and are usually attributed to competition between the FOR (**Equation 1**) and the Cannizzaro reaction (CR; **Equation 2**), based on the assumption that the CR exhibits a higher reaction order with respect to HCHO. However, this proposed competition remains unverified, as CR is widely regarded as a liquid-phase process and has typically been reported under strong alkaline or elevated-temperature conditions (e.g., ≥5 M OH^- or ≥55 °C),[35-37] which differ from typical electrochemical conditions. Nevertheless, no systematic study has been conducted to validate this hypothesis. To explore this, we first demonstrate that CR in our system is not purely homogeneous, but rather a hybrid process involving both homogeneous and heterogeneous pathways, with the latter potentially competing with FOR for active sites on the Cu/Cu_2O surface (**Fig. S23**). Next, we conducted CA testing at 0 V_{RHE} across the same range of electrolyte concentrations and measured the formate production. Based on the response current, we derived the amount of formate generated via FOR, which allowed us to differentiate the contributions of the FOR and CR pathways and clarify their competitive relationship. The results reveal that higher KOH concentrations promote FOR, while elevated HCHO concentrations favor CR (**Table S2**). In addition, the peak point, defined as the HCHO concentration at which the highest FOR activity is observed within the tested range at a given KOH level, varies with alkalinity and increases as the KOH concentration rises (**Fig. 4A**).

A similar trend is observed at a higher potential (0.18 V_{RHE}); however, the peak point shifts to a higher HCHO concentration under the same KOH condition (**Fig. 4B**). This upshift can be attributed to enhanced anion transport at higher applied potentials, which increases OH^- accessibility at the anode surface under comparable bulk basicity (**Fig. 4C**) and facilitates FOR.[38,39] Our findings highlight that FOR activity can be enhanced through electrolyte tuning instead of electrode engineering, with increased alkalinity sustaining performance at high current densities operation. The promoting effect of OH^- is likely related to the conversion of HCHO to deprotonated gem-diol under alkaline conditions,[25,26,29] as deprotonated gem-diol has been proposed as a thermodynamically favorable intermediate in the FOR based on previous DFT studies.[26,27] To substantiate this, we performed a thermodynamic speciation analysis of HCHO in alkaline conditions. The analysis demonstrates that higher KOH concentrations strongly facilitate the formation of the deprotonated gem-diol species, which is the primary electroactive reactant for the FOR (**Supplementary Text 4**). This thermodynamic trend aligns with our experimental observations, providing a robust basis for the enhanced FOR performance at high alkalinity.

Performance Benchmarking and Energy Analysis of the BCE-FOR System

We evaluated the system performance under an industrially relevant current density of 200 mA cm^{-2} (**Fig. 5A**). When using a commercial BPM (c-BPM), the BCE-FOR configuration exhibited a notable voltage reduction of 1.6 V compared to the BCE-OER system, primarily due to the thermodynamic potential difference between OER and FOR (theoretically 1.45 V; **Fig. S1**). Cell voltage can be further improved by introducing the synthetic BPM (s-BPM). The BCE-FOR system with s-BPM exhibited stable operation at a full-cell voltage of 1.7 V, while maintaining $99.5 \pm 0.5\%$ FE for CO generation at the cathode and $101.4 \pm 1.5\%$ FE for H_2 generation at the anode throughout an 8-hour electrolysis. The reduction in cell voltage can be primarily attributed to the catalyst layer design at the BPM junction and the use of highly conductive polymer layers,

which together facilitates water dissociation and enhances ionic transport (**Supplementary Text 5**).[40,41] The resulting gas streams from both electrodes feature an H_2:CO ratio near 1, meeting the industrial syngas requirements. It is worth noting that our BCE-FOR system operates at a low cell voltage comparable to that of state-of-the-art water electrolyzers (< 2 V),[42] enabling compatibility with existing water electrolysis infrastructure without concerns about high-voltage-induced side reactions or adverse effects. Moreover, no discernible changes in voltage or product distribution were observed after refreshing the electrolyte.

The energy analysis reveals that the levelized energy requirement of the BCE-FOR electrolyzer is lower than that of conventional electrolyzers (**Fig. S24**). However, the energy consumption associated with BoP operations, as well as the cost of purchasing HCHO, constitute the dominant component of the overall operational expenditure (OPEX) in this process. Due to the uncertainty associated with BoP energy conditions, particularly under scale-up scenarios, this contribution has been analyzed separately (**Fig. 5B, S25 and Supplementary Text 6**). The large BoP energy demand includes the requirement of an additional conditioning unit upstream of the cathode (BCE) to achieve the desired bicarbonate concentration and a separation-regeneration scheme downstream to recover the products and recycle the unused reactants.[43] The production of bicarbonates is energetically feasible when CO_2 is captured from concentrated point sources such as flue gas and concentration could be achieved through alkali-stable high throughput membrane-based separation units to minimize the energy requirement.[43,44] The OH^- flux from the BPM is insufficient to compensate for the OH^- consumption required during FOR, leading to gradual acidification of the anolyte. This issue can be mitigated by BPM electrodialysis (BPMED),[45] which simultaneously separates formate from the anolyte as formic acid and regenerates KOH. Evolution of gaseous CO_2 in the cathode also necessitates a larger pressure-swing adsorption unit to recover the CO_2 and purify the syngas stream. The downstream separation train, particularly the BPMED

unit, is the dominant contributor to the overall energy demand of the BCE-FOR process. Although the combined energy consumption for upstream capture, conditioning, and electrolyzer conversion is only 5.8 MWh ton^{-1}_{syngas}, inclusion of the downstream separations increases the total process energy requirement to approximately 20 MWh ton^{-1}_{syngas}. At the current stage of development, this approach has yet to surpass conventional petrochemical syngas production routes (6.4 MWh ton^{-1}_{syngas}) in terms of energy demand. More broadly, the minimum levelized energy required to produce syngas via the BCE-FOR system varies highly depending on the upstream/downstream processes (**Fig. 5B**) and the overall economics will depend on both BoP energy and consumable material costs, particularly aldehyde and electrolyte management. Nevertheless, the full-cell syngas production system proposed in this work demonstrates promising performance in terms of H_2:CO ratio, cell voltage, and total throughput, compared to other reported electrochemical approaches (**Fig. 5C; Table S4**).

Importantly, the anodic product stream creates a clear co-product lever when the system is integrated with acid recovery via BPMED: in our base design the FOR anode produces a substantial formate stream that can be recovered as formic acid, providing an additional value stream rather than a disposal burden. Across the scenarios in **Fig. S25 and Table S3**, this recovery step remains comparatively favorable because it monetizes an otherwise "embedded" anodic output and helps offset the added consumable requirement associated with aldehyde feed. In this study, formaldehyde is employed as a model molecule to benchmark the performance limits of FOR-assisted electrolysis and to leverage its favorable kinetics/thermodynamics. However, FOR is not limited to formaldehyde: biomass-derived oxygenates such as furfural and related platform molecules have been proposed as alternative anodic substrates within broader biomass valorization schemes (**Supplementary Text 7**). At the same time, scalability considerations differ substantially across candidate substrates; formaldehyde is a high-volume commodity chemical produced and

consumed at multi-million-ton-per-year scale, whereas furfural markets are typically reported at hundreds of thousands of tons per year, implying markedly different supply-chain and deployment constraints. Consequently, the most economically compelling FOR implementations may involve either (i) leveraging abundant, low-cost oxygenate streams (including biomass-derived intermediates) where available, or (ii) using large-market substrates (e.g., formaldehyde) when the objective is grid-scale operation and the anodic co-product (formate/formic acid) can be efficiently recovered and monetized.

At today's state of the art, the fully integrated BCE-FOR syngas pathway is not yet uniformly competitive on a process system basis, primarily because overall economics are dominated by BoP and downstream processing penalties rather than by the cell itself. This is reflected in the pessimistic case (patterned bars), where the minimum selling price (MSP) rises to roughly 4–8 USD kg_{syngas}^{-1} depending on the H_2:CO operating mode and whether external H_2 makeup is required (**Fig. S25C**). In this analysis, we evaluate the MSP of syngas under the assumption of spot market pricing for both purchased formaldehyde and the recovered formate as 1 M formic acid **(Supplementary Text 6**). The corresponding capital and operating cost burdens are likewise concentrated in downstream and BoP contributions (**Fig. S25A, B**), indicating that the principal limitation is not the feasibility of the electrochemical step, but the current cost structure of the integrated plant. Crucially, the same breakdown also shows a credible pathway to feasibility as electrolyzer and BoP costs decline. Under the optimistic assumptions (solid bars), the MSP compresses to approximately 0.6–1.5 USD kg_{syngas}^{-1}, again depending on operating mode and H_2 makeup needs (**Fig. S25C**), with the reductions driven by lower stack/BoP capital intensity and reduced utility burdens (**Fig. S25A, B**). In other words, the scenario analysis indicates that continued declines in electrolyzer CAPEX, improved durability, and BoP cost decreases can shift the process into a regime where FOR-assisted operation becomes economically attractive –

especially when the anodic formate can be efficiently recovered and sold as formic acid rather than treated as a low-value byproduct. This work sparks new perspectives for the development of electrochemical syngas production and demonstrates the potential to serve as a viable alternative to petrochemical routes through continued advances in system integration.

Conclusions

We demonstrate an integrated electrochemical syngas production platform that couples BCE with FOR in a BPM-MEA. By enabling both electrodes to generate syngas components, this architecture overcomes the intrinsic productivity limitation of OER-based systems and doubles the theoretical molar yield per unit charge. The system produces syngas with a targeted 1:1 H_2:CO directly within a single reactor. The BCE-FOR electrolyzer operates stably at an industrially relevant current density of 200 mA cm^{-2} with a low full-cell voltage of 1.7 V, maintaining near-unity FE for CO and H_2 production over 8 hours. These performance gains reduce the levelized energy requirement for syngas production by 45%–61% relative to conventional gaseous CO_2E-OER and BCE-OER platforms. The use of bicarbonate feedstocks further enables direct integration with carbon capture processes. We further elucidate the role of Cu anode active sites and electrolyte composition in sustaining efficient FOR and anodic hydrogen production at high current densities. Together, these findings establish a generalizable strategy for replacing OER with value-generating anode reactions. While challenges remain in aldehyde sourcing, durability, and system integration, this work provides a new paradigm for energy-efficient, CO_2-derived syngas production.

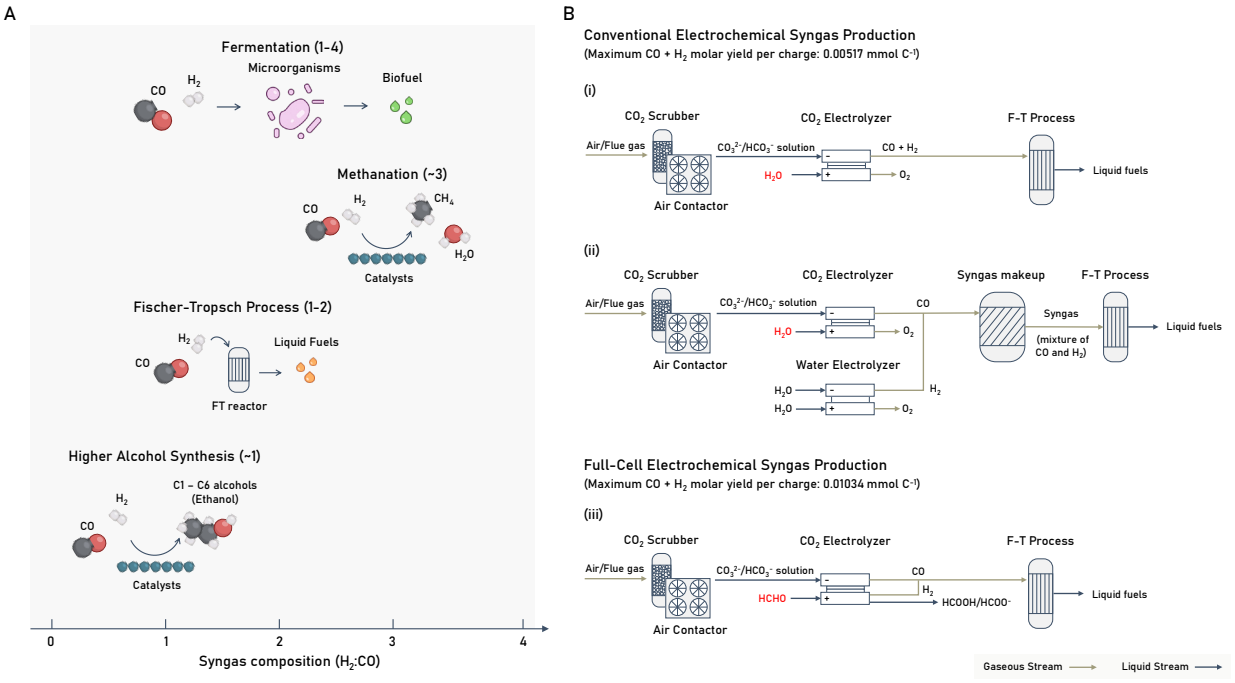

Fig. 1. Syngas composition and utilization pathways with electrochemical production strategies. (A) Various downstream chemical synthesis routes enabled by syngas with different H_2:CO ratios. **(B)** Schematic comparison between conventional and full-cell electrochemical syngas production systems. Conventional systems consist of (i) a single CO_2 electrolyzer that produces both CO and H_2 at the cathode, and (ii) a tandem system combining a CO_2 electrolyzer (for CO production) and a separate water electrolyzer (for H_2 generation). The full-cell configuration (iii) couples CO_2 reduction with aldehyde oxidation, enabling co-generation of CO (at cathode) and H_2 (at anode) within one reactor. This approach doubles the molar yield per charge compared to conventional systems. The syngas makeup step refers to downstream adjustment of the H_2:CO ratio by blending gaseous streams from coupled reactors. F-T process refers to Fischer-Tropsch process.

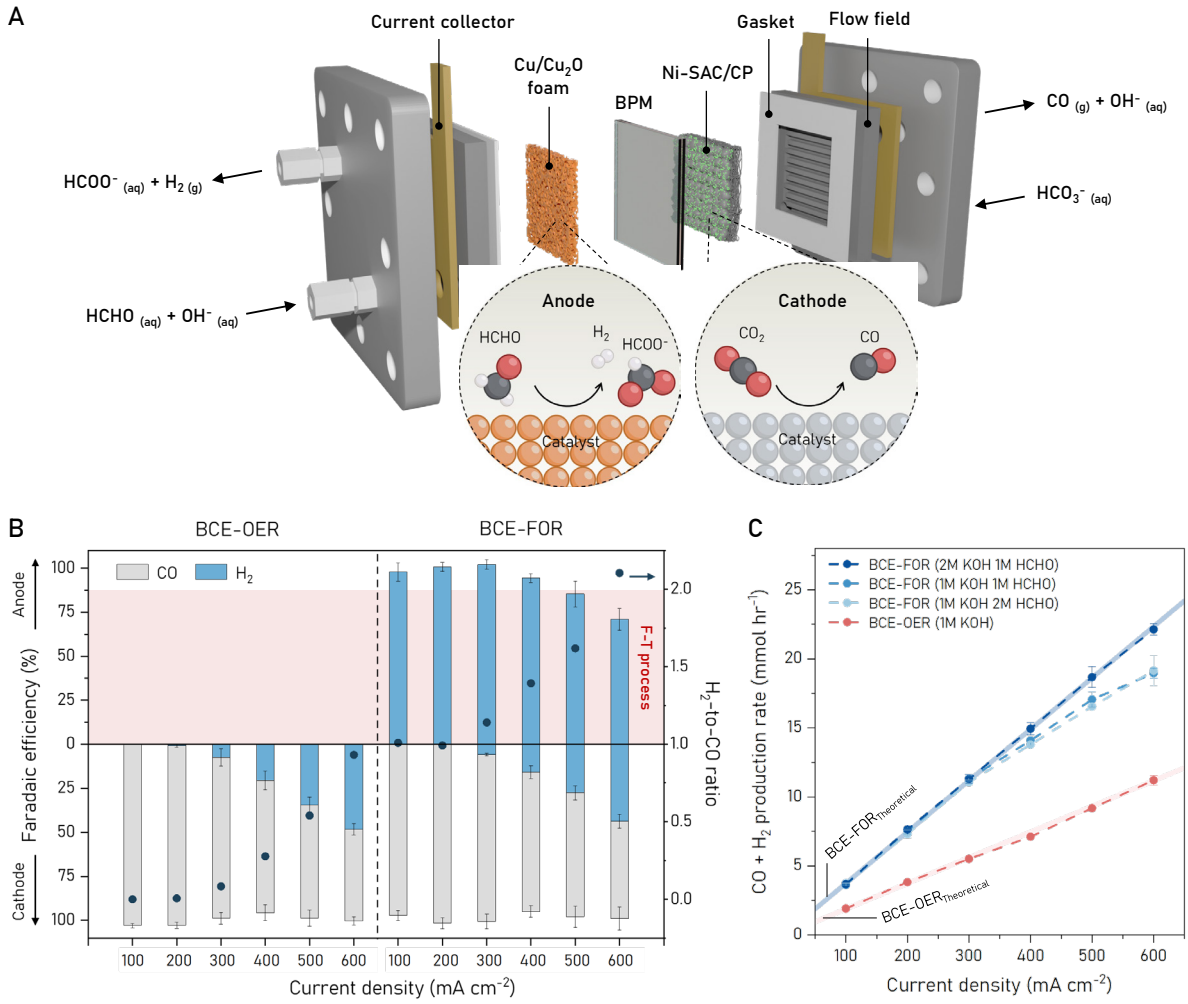

Fig. 2. Coupled bicarbonate electrolysis and formaldehyde oxidation for full-cell syngas generation. (A) Schematic of a MEA electrolyzer integrating bicarbonate electrolysis (BCE) with the formaldehyde oxidation reaction (FOR). The system uses a bipolar membrane (BPM) to separate cathode and anode, with Ni single-atom catalyst (Ni-SAC) supported on carbon paper at the cathode and Cu/Cu_2O foam at the anode. **(B)** Faradaic efficiencies for CO and H_2 and corresponding H_2-to-CO ratios under various current densities (100-600 mA cm^{-2}) in the BCE-FOR and BCE-OER (oxygen evolution reaction) configurations. Left y-axis: Faradaic efficiencies are plotted with cathodic products (CO and H_2) shown as downward bars, and anodic products shown as upward bars on the same x-axis. Right y-axis: Dot markers represent the resulting H_2-to-CO ratio of the syngas. The red shaded area highlights the ideal H_2:CO ratio range for Fischer-Tropsch process. **(C)** Total syngas (CO + H_2) production rate under different electrolyte compositions for BCE-FOR (2 M KOH + 1 M HCHO, 1 M KOH + 1 M HCHO, and 1 M KOH +

2 M HCHO) compared to BCE-OER (1 M KOH). Solid and dashed lines represent theoretical and experimental values, respectively. Error bars indicate standard deviations from three independent measurements.

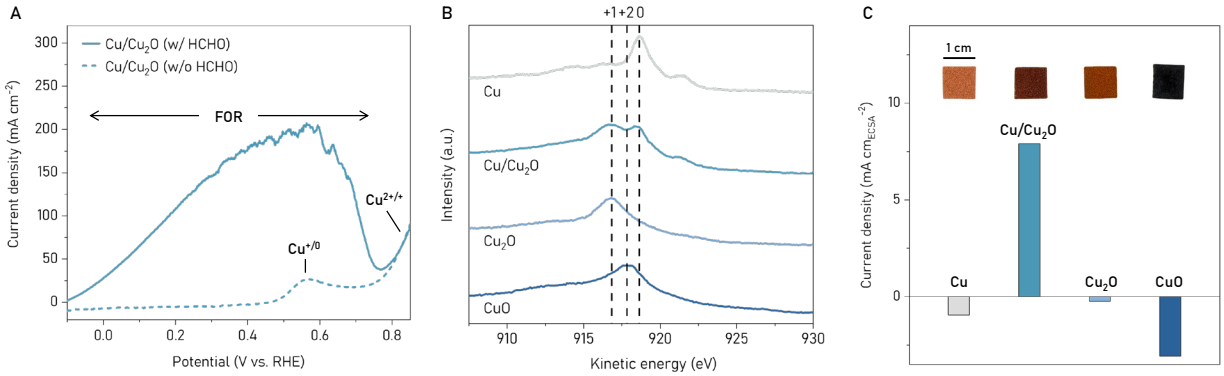

Fig. 3. Formaldehyde oxidation reaction (FOR) activity on Cu-based anodes. **(A)** Linear sweep voltammetry (LSV) of Cu/Cu_2O electrodes in 1 M KOH with (solid line) and without (dashed line) 200 mM formaldehyde. The sharp anodic current observed in the presence of formaldehyde indicates FOR activity. In the absence of formaldehyde, a peak near 0.55 V_{RHE} corresponds to the Cu^0 to Cu^+ oxidation process. **(B)** Auger Cu LMM spectra showing surface valance states of Cu-based electrodes. The kinetic energy positions reveal that Cu, Cu_2O, and CuO contain only Cu^0, Cu^+, and Cu^{2+}, respectively, while Cu/Cu_2O exhibits a combination of Cu^0 and Cu^+. **(C)** FOR current densities normalized to electrochemical surface area (ECSA) for Cu, Cu/Cu_2O, Cu_2O, and CuO electrodes. Inset shows corresponding optical images of the electrodes.

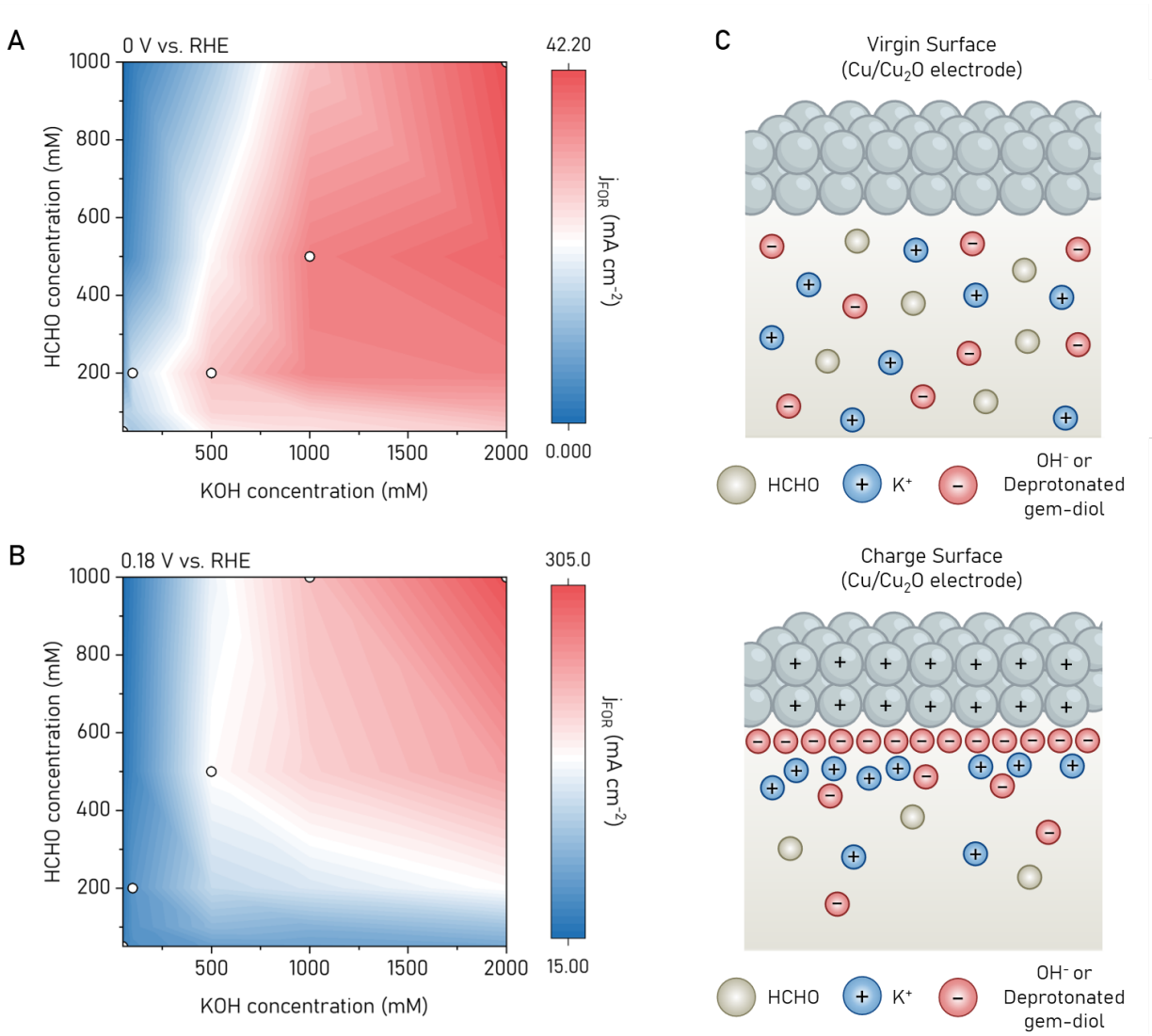

Fig. 4. Effect of electrolyte composition on formaldehyde oxidation reaction (FOR) activity. **(A–B)** Contour plots of FOR activity as a function of KOH and HCHO concentrations at **(A)** 0 V_{RHE} and **(B)** 0.18 V_{RHE}. Electrolyte compositions range from 50 to 2000 mM for KOH and 50 to 1000 mM for HCHO. For each fixed KOH concentration, dots (peak points) denote the HCHO concentration that results in the highest FOR activity within the tested range. **(C)** Schematic illustration of the interfacial environment near the Cu/Cu_2O electrode at open-circuit (virgin surface) and under bias (charged surface). At higher applied potential, the enhanced transport of anions (i.e., OH^- and deprotonated gem-diol) toward the surface enhances the availability of reactive species for formaldehyde oxidation reaction.

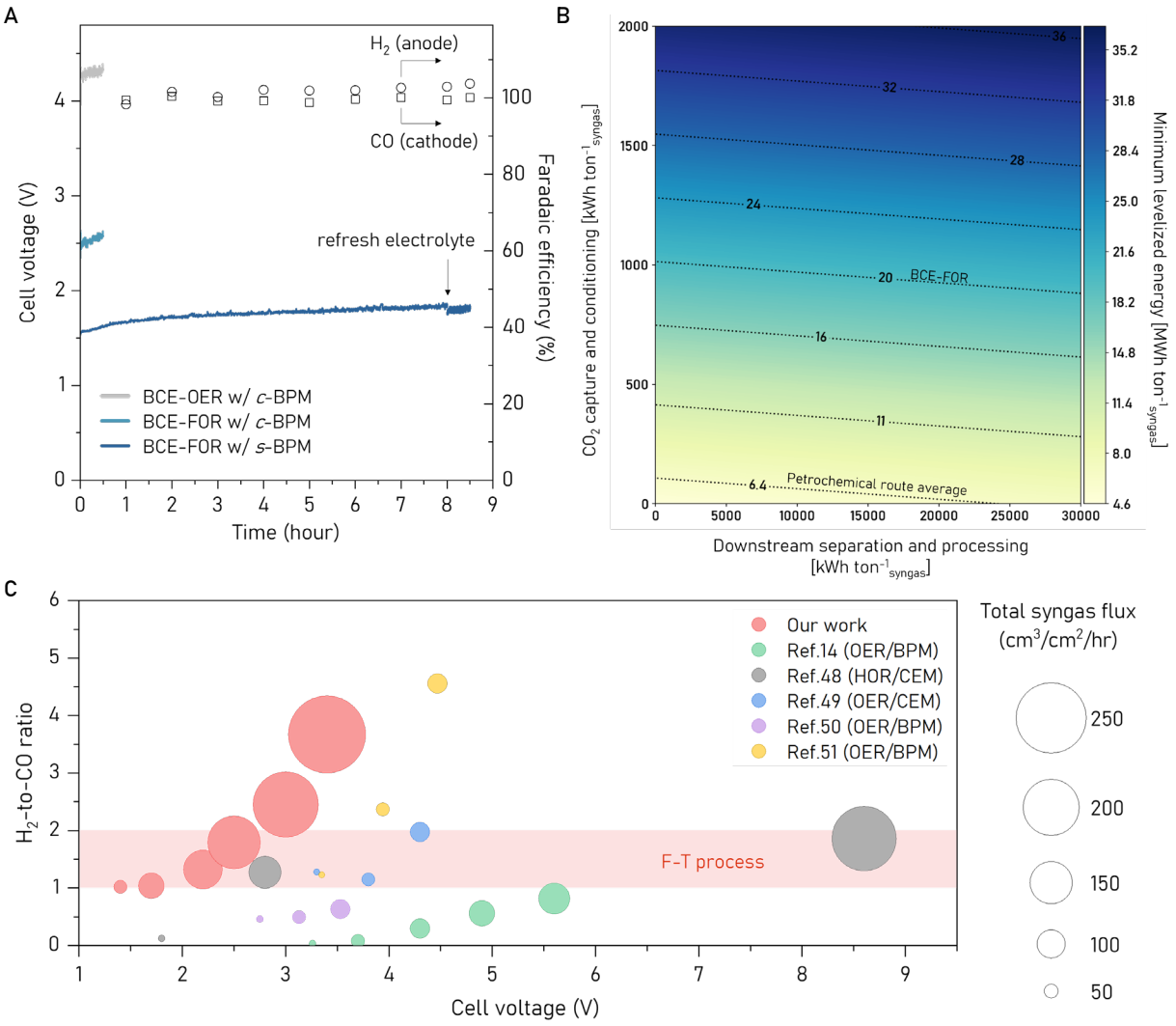

Fig. 5. Durability, energy analysis, and benchmarking of the BCE-FOR system for electrochemical syngas production. (A) Comparison of full-cell voltages for BCE-FOR and BCE-OER systems using c-BPM and s-BPM during 30 min electrolysis. Stability of BCE-FOR with s-BPM over 8 hours, with corresponding CO and H_2 Faradaic efficiencies plotted on the right y-axis. **(B)** Minimum levelized energy required to produce syngas via the BCE-FOR process under varying balance-of-plant (BoP) energy conditions. The petrochemical syngas production route average is represented by the 6.4 MWh ton^{-1}_{syngas} line, based on the Refs. 46, 47. **(C)** Benchmark comparison of syngas ratio (H_2:CO) versus cell voltage across various reported systems and this work. Bubble size corresponds to total syngas (H_2 + CO) flux, and the red shaded area denotes the ideal syngas ratio range for the Fischer-Tropsch (F-T) process. The legend indicates literature references, annotated by anodic reaction and membrane type (e.g., OER/BPM, HOR/CEM). All

syngas ratios were calculated based on experimental data from the corresponding references. Experimental conditions: This work, Refs. 14, 49, 50, and 51 were conducted at ambient pressure and room temperature; Ref. 48 was performed at 3.5 atm and room temperature. CEM: cation exchange membrane; HOR: hydrogen oxidation reaction.

Reference

1. P. De Luna, C. Hahn, D. Higgins, S. A. Jaffer, T. F. Jaramillo and E. H. Sargent, *Science*, 2019, **364**, eaav3506.
2. Carbon Monoxide Market Size, https://www.fortunebusinessinsights.com/carbon-monoxide-market-105343).
3. N. Mahinpey, A. Farooqui, A. Abdalla and K. Asghari, in *Advances in Synthesis Gas : Methods, Technologies and Applications*, eds. M. R. Rahimpour, M. A. Makarem and M. Meshksar, Elsevier, 2023, vol. 3, pp. 289-319.
4. M. Bachmann, S. Völker, J. Kleinekorte and A. Bardow, *ACS Sustain. Chem. Eng.*, 2023, **11**, 5356-5366.
5. C. P. O'Brien, R. K. Miao, A. Shayesteh Zeraati, G. Lee, E. H. Sargent and D. Sinton, *Chem. Rev.*, 2024, **124**, 3648-3693.
6. H. Shin, K. U. Hansen and F. Jiao, *Nat. Sustain.*, 2021, **4**, 911-919.
7. B. Belsa, L. Xia and F. P. García de Arquer, *ACS Energy Lett.*, 2024, **9**, 4293-4305.
8. M. Jouny, G. S. Hutchings and F. Jiao, *Nat. Catal.*, 2019, **2**, 1062-1070.
9. A. Raya-Imbernón, A. A. Samu, S. Barwe, G. Cusati, T. Fődi, B. M. Hepp and C. Janáky, *ACS Energy Lett.*, 2024, **9**, 288-297.
10. Z. Huang, R. G. Grim, J. A. Schaidle and L. Tao, *Energy Environ. Sci.*, 2021, **14**, 3664-3678.
11. S. Hernández, M. Amin Farkhondehfal, F. Sastre, M. Makkee, G. Saracco and N. Russo, *Green Chem.*, 2017, **19**, 2326-2346.
12. M. B. Ross, Y. Li, P. De Luna, D. Kim, E. H. Sargent and P. Yang, *Joule*, 2019, **3**, 257-264.
13. Z. Qi, A. R. Kashi, A. K. Buckley, J. S. Miller, J. Ye, M. M. Biener, A. C. Foucher, E. A. Stach, S. Ma, K. P. Kuhl and J. Biener, *J. Phys. Chem. C*, 2022, **126**, 19637-19646.
14. H. Song, C. A. Fernández, H. Choi, P.-W. Huang, J. Oh and M. C. Hatzell, *Energy Environ. Sci.*, 2024, **17**, 3570-3579.
15. M. R. Gerhardt, L. M. Pant, J. C. Bui, A. R. Crothers, V. M. Ehlinger, J. C. Fornaciari, J. Liu and A. Z. Weber, *J. Electrochem. Soc.*, 2021, **168**, 074503.
16. S. Popović, M. Smiljanić, P. Jovanovič, J. Vavra, R. Buonsanti and N. Hodnik, *Angew. Chem.-Int. Edit.*, 2020, **59**, 14736-14746.
17. L. Castanheira, L. Dubau, M. Mermoux, G. Berthomé, N. Caqué, E. Rossinot, M. Chatenet and F. Maillard, *ACS Catal.*, 2014, **4**, 2258-2267.
18. B. Zhang, L. Wang, Z. Cao, S. M. Kozlov, F. P. García de Arquer, C. T. Dinh, J. Li, Z. Wang, X. Zheng, L. Zhang, Y. Wen, O. Voznyy, R. Comin, P. De Luna, T. Regier, W. Bi, E. E. Alp, C.-W. Pao, L. Zheng, Y. Hu, Y. Ji, Y. Li, Y. Zhang, L. Cavallo, H. Peng and E. H. Sargent, *Nat. Catal.*, 2020, **3**, 985-992.
19. C. Liang, R. Zhao, T. Chen, Y. Luo, J. Hu, P. Qi and W. Ding, *Adv. Sci.*, 2024, **11**, 2308958.
20. S. Wang, Y. Lin, Y. Li, Z. Tian, Y. Wang, Z. Lu, B. Ni, K. Jiang, H. Yu, S. Wang, H. Yin and L. Chen, *Nat. Nanotechnol.*, 2025, **20**, 646-655.
21. Y. C. Li, G. Lee, T. Yuan, Y. Wang, D.-H. Nam, Z. Wang, F. P. García de Arquer, Y. Lum, C.-T. Dinh, O. Voznyy and E. H. Sargent, *ACS Energy Lett.*, 2019, **4**, 1427-1431.
22. T. Li, E. W. Lees, M. Goldman, D. A. Salvatore, D. M. Weekes and C. P. Berlinguette, *Joule*, 2019, **3**, 1487-1497.
23. Z. Zhang, E. W. Lees, F. Habibzadeh, D. A. Salvatore, S. Ren, G. L. Simpson, D. G. Wheeler, A. Liu and C. P. Berlinguette, *Energy Environ. Sci.*, 2022, **15**, 705-713.
24. D. Salvatore and C. P. Berlinguette, *ACS Energy Lett.*, 2020, **5**, 215-220.

25. T. Wang, L. Tao, X. Zhu, C. Chen, W. Chen, S. Du, Y. Zhou, B. Zhou, D. Wang, C. Xie, P. Long, W. Li, Y. Wang, R. Chen, Y. Zou, X.-Z. Fu, Y. Li, X. Duan and S. Wang, *Nat. Catal.*, 2022, **5**, 66-73.
26. Y. Pan, Y. Li, C.-L. Dong, Y.-C. Huang, J. Wu, J. Shi, Y. Lu, M. Yang, S. Wang and Y. Zou, *Chem*, 2023, **9**, 963-977.
27. G. Li, G. Han, L. Wang, X. Cui, N. K. Moehring, P. R. Kidambi, D.-e. Jiang and Y. Sun, *Nat. Commun.*, 2023, **14**, 525.
28. H. Choi, M. G. Ha, J. Suh, C. Lim, B. Kim, S. E. Wang, J. Y. Lee, H.-S. Oh and J. Oh, *Appl. Catal. B-Environ. Energy*, 2024, **355**, 124192.
29. H. Liu, N. Agrawal, A. Ganguly, Y. Chen, J. Lee, J. Yu, W. Huang, M. Mba Wright, M. J. Janik and W. Li, *Energy Environ. Sci.*, 2022, **15**, 4175-4189.
30. S.-Q. Liu, M.-R. Gao, S. Wu, R. Feng, Y. Wang, L. Cui, Y. Guo, X.-Z. Fu and J.-L. Luo, *Energy Environ. Sci.*, 2023, **16**, 5305-5314.
31. X. Gao, Y. Pan, J. Qiu, J. Peng, S. Wang and Y. Zou, *Adv. Funct. Mater.*, 2025, **35**, 2417545.
32. M. Yang, Y. Jiang, C.-L. Dong, L. Xu, Y. Huang, S. Leng, Y. Wu, Y. Luo, W. Chen, T. T. T. Nga, S. Wang and Y. Zou, *Nat. Commun.*, 2024, **15**, 9852.
33. J. Timoshenko, A. Bergmann, C. Rettenmaier, A. Herzog, R. M. Arán-Ais, H. S. Jeon, F. T. Haase, U. Hejral, P. Grosse, S. Kühl, E. M. Davis, J. Tian, O. Magnussen and B. Roldan Cuenya, *Nat. Catal.*, 2022, **5**, 259-267.
34. M. Yang, Y. Li, C.-L. Dong, S. Li, L. Xu, W. Chen, J. Wu, Y. Lu, Y. Pan, Y. Wu, Y. Luo, Y.-C. Huang, S. Wang and Y. Zou, *Adv. Mater.*, 2023, **35**, 2304203.
35. M. S. Kharasch and M. Foy, *J. Am. Chem. Soc.*, 1935, **57**, 1510-1510.
36. W. C. Wilson, in *Organic Syntheses*, 2003, pp. 44-44.
37. K. Bowden, F. A. El-Kaissi and R. J. Ranson, *J. Chem. Soc.-Perkin Trans. 2*, 1990, 2089-2092.
38. S. R. Alfarano, S. Pezzotti, C. J. Stein, Z. Lin, F. Sebastiani, S. Funke, C. Hoberg, I. Kolling, C. Y. Ma, K. Mauelshagen, T. Ockelmann, G. Schwaab, L. Fu, J.-B. Brubach, P. Roy, M. Head-Gordon, K. Tschulik, M.-P. Gaigeot and M. Havenith, *Proc. Natl. Acad. Sci. U. S. A.*, 2021, **118**, e2108568118.
39. K. Doblhoff-Dier and M. T. M. Koper, *J. Phys. Chem. C*, 2021, **125**, 16664-16673.
40. S. Sasmal, L. Chen, P. V. Sarma, O. T. Vulpin, C. R. Simons, K. M. Wells, R. J. Spontak and S. W. Boettcher, *Nat. Mater.*, 2024, **23**, 1421-1427.
41. C. Espinoza, D. Kitto and J. Kamcev, *ACS Appl. Polym. Mater.*, 2023, **5**, 10324-10333.
42. N. Du, C. Roy, R. Peach, M. Turnbull, S. Thiele and C. Bock, *Chem. Rev.*, 2022, **122**, 11830-11895.
43. A. Venkataraman, H. Song, V. D. Brandão, C. Ma, M. S. Casajus, C. A. Fernandez Otero, C. Sievers, M. C. Hatzell, S. S. Bhargava, S. S. Arora, C. Villa, S. Dhingra and S. Nair, *Nat. Chem. Eng.*, 2024, **1**, 710-723.
44. Z. Wang, C. Ma, C. Xu, S. A. Sinquefield, M. L. Shofner and S. Nair, *Nat. Sustain.*, 2021, **4**, 402-408.
45. J. S. J. Ferrer, S. Laborie, G. Durand and M. Rakib, *J. Membr. Sci.*, 2006, **280**, 509-516.
46. M. Escribà-Gelonch, J. Osorio-Tejada, L. Yu, B. Wanten, A. Bogaerts and V. Hessel, *Energy Environ. Sci.*, 2025, **18**, 6043-6062.
47. L. Zheng, M. Ambrosetti, A. Beretta, G. Groppi and E. Tronconi, *J. Chem. Eng.*, 2023, **466**, 143154.
48. Z. Zhang, E. W. Lees, S. Ren, B. A. W. Mowbray, A. Huang and C. P. Berlinguette, *ACS Cent. Sci.*, 2022, **8**, 749-755.

49. Y. C. Xiao, C. M. Gabardo, S. Liu, G. Lee, Y. Zhao, C. P. O'Brien, R. K. Miao, Y. Xu, J. P. Edwards, M. Fan, J. E. Huang, J. Li, P. Papangelakis, T. Alkayyali, A. Sedighian Rasouli, J. Zhang, E. H. Sargent and D. Sinton, *EES catal.*, 2023, **1**, 54-61.
50. B. Zhou, H. Liu, G. Su, H. Shin, X.-Y. Li, H. Ze, Y. Liang, B. Peng, W. Ni, Y. Chen, W. Zhu, C. Yu, Y. Chen, P. Ou, K. Xie and E. H. Sargent, *Joule*, 2025, **9**.
51. D. He, X. Ma, H. Zhou, Y. Zhang and Y. Wu, *Joule*, 2025, **9**, 101806.

Acknowledgments

The authors thank Dr. Andrew J. Medford from Georgia Institute of Technology for the insightful discussion. During the preparation of this work the authors used ChatGPT for grammar check. After using this tool, the authors reviewed and edited the content as needed and took full responsibility for the content of the publication. **Funding:** The information, data, or work presented herein was funded in part by the Advanced Research Projects Agency-Energy (ARPA-E), U.S. Department of Energy, under Award Number DE-AR0001949. This work was supported by the National Research Foundation of Korea (NRF) grant funded by the Korea government (MSIT) (Nos. RS-2024-00406517, RS-2021-NR060090, and RS-2024-00435493).

Author Contributions

Conceptualization: PH, HC, JO, HS, and MCH Investigation: PH, HC, AV, VO, CART, DACH, TZ, ERY, and HS Visualization: PH, and HC Funding acquisition: KBH, SWB, SN, JO, and MCH Supervision: MCH Writing – original draft: PH, HC, and HS Writing – review & editing: PH, HC, AV, VO, CART, DACH, YZ, ERY, KBH, SWB, SN, JO, HS, and MCH.

Competing Interests: Authors declare that they have no competing interests.

Data and materials availability: All data are available in the main text or the supplementary materials. Additional raw data, analysis code, and experimental procedures can be obtained from the corresponding author upon reasonable request.

Broader Context

Syngas (H_2 and CO) is a foundational intermediate for fuels, chemicals, and emerging sustainable aviation fuel pathways, yet its production remains dominated by fossil-derived processes with significant carbon emissions. Electrochemical routes using captured CO_2 offer a promising alternative, but current CO_2 electrolyzer platforms are constrained by high energy consumption, limited syngas yield per unit charge, and poor integration between hydrogen and carbon monoxide production. In particular, the oxygen evolution reaction at the anode imposes a fundamental energetic penalty while contributing no value to the target product stream. This work addresses these challenges by rethinking the anodic reaction and electrolyte architecture in CO_2-derived syngas production. By coupling bicarbonate electrolysis with aldehyde oxidation in a bipolar membrane electrode assembly, both electrodes actively generate syngas components, enabling doubled molar productivity per coulomb and substantially reduced energy input. Beyond improving efficiency, this strategy directly interfaces with carbon capture-derived bicarbonate feeds and produces an industrially relevant H_2:CO ratio within a single reactor. The demonstrated approach highlights how alternative anodic chemistries can unlock new design principles for low-carbon electrochemical manufacturing and accelerate the deployment of CO_2 utilization technologies at scale.

TOC

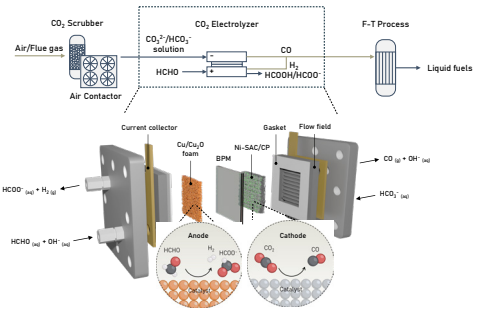

A bipolar membrane electrolyzer coupling bicarbonate electrolysis with formaldehyde oxidation directly produces syngas (H_2:CO = 1) at 1.7 V and 200 mA cm^{-2} with 200% combined Faradaic efficiency.